MOX–Report No. 30/2009

On computing upper and lower bounds on the outputs of linear elasticity problems approximated by the smoothed finite element method

Z. C. Xuan, T. Lassila, Gianluigi Rozza,
Alfio Quarteroni

MOX, Dipartimento di Matematica "F. Brioschi"
Politecnico di Milano, Via Bonardi 9 - 20133 Milano (Italy)

mox@mate.polimi.it http://mox.polimi.it

On computing upper and lower bounds on the outputs of linear elasticity problems approximated by the smoothed finite element method

Z.C. Xuan[♯], T. Lassila[§], G. Rozza[⋆,*], A. Quarteroni[⋆,†]

October 8, 2009

[♯] Department of Computer Science, Tianjin University of Technology and Education, Tianjin 300222, China.
[§] Institute of Mathematics, Helsinki University of Technology, P.O. Box 1100, FI-02015 TKK, Finland.
[⋆] Modeling and Scientific Computing, IACS-CMCS, École Polytechnique Fédérale de Lausanne, EPFL, Station 8, CH-1015 Lausanne, Switzerland.
[†] MOX– Modellistica e Calcolo Scientifico, Dipartimento di Matematica "F. Brioschi" Politecnico di Milano, via Bonardi 9, 20133 Milano, Italy

Keywords: error bounds; linear elasticity; output; finite element method; smoothed finite element method

Abstract

Verification of the computation of local quantities of interest, e.g. the displacements at a point, the stresses in a local area and the stress intensity factors at crack tips, plays an important role in improving the structural design for safety. In this paper, the smoothed finite element method (SFEM) is used for finding upper and lower bounds on the local quantities of interest that are outputs of the displacement field for linear elasticity problems, based on bounds on strain energy in both the primal and dual problems. One important feature of SFEM is that it bounds the strain energy of the structure from above without needing the solutions of different subproblems that are based on elements or patches but only requires the direct finite element computation. Upper and lower bounds on two linear outputs and one quadratic output related with elasticity – the local reaction, the local displacement, and the J-integral – are computed by the proposed method in two different examples. Some issues with SFEM that remain to be resolved are also discussed.

[*]Corresponding Author, E-mail: gianluigi.rozza@epfl.ch

1 Introduction

Finite element analysis is a common tool in computer aided engineering design. From a theoretical point of view, the approximation produced by FEM lies in a finite-dimensional subspace of the infinite-dimensional space where the exact solution of the problem resides. Typically, no matter how large the finite-dimensional space is, if the exact solution does not live in the finite element space, there will always be a *distance* between the finite element solution and the exact solution. Many a posteriori error estimates for finite element analysis have been established to quantify the error of the computed solution in the energy norm for elliptic partial differential equations [1–4].

Numerical solutions of partial differential equations are often used to determine approximations to quantities of practical interest such as displacements, forces, or stresses. We refer to these quantities as *outputs*. Once a solution has been computed on a given mesh, one is interested in determining the reliability of the approximated outputs. In order to address this question a number of a posteriori error estimation methods have been proposed with the aim of quantifying the functional outputs of practical interest such as displacements or stresses [5–9]. In this paper we will consider the elliptic system of linear elasticity.

A key ingredient to the output bound procedure is the computation of global upper and lower bounds on the total strain energy. It is known already since the early work of de Veubeke [10] that an approximation based on the potential energy principle (displacement method), which uses displacements as variables, will give a lower bound on the global strain energy. Conversely, the complementary energy principle (equilibrium method) that uses stresses as variables will give an upper bound on the global strain energy [11, 12]. The difficulties arising with equilibrium methods are the processing of boundary conditions. The right hand side of the resulting discrete algebraic equation is zero if the displacement is zero on the Dirichlet boundary, and the applied loads cannot be implemented by merely striking out rows and columns of the flexibility equations, which is the usual way in which displacement boundary conditions are implemented in the displacement/stiffness method [13]. Parés et al [9] have presented computable upper and lower bounds on exact outputs. Their method can be regarded as a generalization of the complementary energy principle; however, they did not solve the equation in stress space, but used a displacement approximation to solve local approximate equilibrated stresses in each element. The finite element approximations to the displacement solution were post-processed to yield the so called inter-element hybrid fluxes for the computation of locally equilibrated stress fields. Thus their method can compute an upper bound on the global strain energy.

Recently a modified FEM with strain smoothing, SFEM, has been proposed to solve solid mechanics problems. It has been found that in some situations the strain energy computed by SFEM bounds the exact strain energy from above

[14–16]. This method stems from mesh-free finite element research and was first proposed to develop a stabilized nodal integration scheme for the Galerkin mesh-free method. The aim is to achieve higher efficiency with desired accuracy and convergence properties. A strain smoothing stabilization is introduced to compute nodal strains by a divergence counterpart of a strain spatial averaging. The strain smoothing method avoids evaluating derivatives of mesh-free shape functions at the nodes and thus eliminates spurious modes [17].

A rigorous proof for the upper bound property for the strain energy of the SFEM is still lacking. In [15] a proof was given, but only in the limited case that the exact solution is in the subspace spanned by the nodal shape functions. The authors also presented a proof for the *softening* effect shown by the stiffness matrix of SFEM, while in [18] a theoretical explanation of SFEM was given. A quasi-equilibrium concept was proposed for the four-node quadrilateral elements, meaning that the upper bound property was due to a quasi-equilibrium condition of the stresses in each finite element, which would make their method a kind of equilibrium method. According to our own experience, several issues remain to be solved with SFEM. For example, the upper bound property seems to hold only with sufficiently fine meshes. Also, the choice of SFEM affects the upper bound property and the situation can vary from problem to problem. In this paper we study SFEM and give several properties, which may be useful for proving the upper bound property. We then extend SFEM to compute lower and upper bounds on general linear outputs of linear elasticity. Since SFEM is a general method, some of our results extend beyond elasticity problems.

In Section 2 we introduce the formulation for the lower and upper bounds on linear functionals of elasticity. In Section 3 we briefly describe the SFEM and some properties thereof. In Section 4 some numerical results are reported and commented on; finally some conclusions are drawn in Section 5.

2 Formulation of the upper and lower bounds on linear functionals of displacement

Let us consider a homogeneous elastic body that occupies a bounded region $\Omega \subset \mathbb{R}^d$ and d is the number of spatial dimensions. The boundary of Ω is assumed to be piecewise smooth, and composed of a Dirichlet portion Γ_D and a Neumann portion Γ_N, i.e. $\partial\Omega = \overline{\Gamma_D \cup \Gamma_N}$. As is customary, $\boldsymbol{u} : \Omega \to \mathbb{R}^d$ denotes displacement, $\boldsymbol{b}$ represents a body force, and $\boldsymbol{t}$ the boundary traction. The stress $\boldsymbol{\sigma}$ in matrix form is related to a strain $\boldsymbol{\varepsilon}(\boldsymbol{u}) = \boldsymbol{D}\boldsymbol{u}$ via a linear constitutive law, i.e., $\boldsymbol{\sigma} = \boldsymbol{E}\boldsymbol{\varepsilon}(\boldsymbol{u})$, where $\boldsymbol{D}$ is the differential operator matrix and $\boldsymbol{E}$ is the elastic moduli matrix. The weak form of the elasticity equation reads: find $\boldsymbol{u}$ in $\mathscr{U}$ such that

$$\int_\Omega \boldsymbol{\varepsilon}^T(\boldsymbol{u})\boldsymbol{E}\boldsymbol{\varepsilon}(\boldsymbol{v})\, d\Omega = \int_\Omega \boldsymbol{b}^T\boldsymbol{v}\, d\Omega + \int_{\Gamma_N} \boldsymbol{t}^T\boldsymbol{v}\, d\Gamma \quad \forall \boldsymbol{v} \in \mathscr{V}, \tag{1}$$

in which $\mathscr{U} = \{\boldsymbol{v} \in (H^1(\Omega))^d \mid \boldsymbol{u} = \boldsymbol{u}_D \text{ on } \Gamma_D\}$ and $\mathscr{V} = \{\boldsymbol{v} \in (H^1(\Omega))^d \mid \boldsymbol{v} = \boldsymbol{0} \text{ on } \Gamma_D\}$ are the usual solution and test spaces respectively, and $\boldsymbol{u}_D$ is the imposed boundary displacements. The notation $H^1(\Omega)$ denotes the usual Sobolev space. The energy norm associated with the bilinear form $\int_\Omega \boldsymbol{\varepsilon}^T(\cdot)\boldsymbol{E}\boldsymbol{\varepsilon}(\cdot)\, d\Omega$ is defined as

$$||\boldsymbol{u}||^2 = \int_\Omega \boldsymbol{\varepsilon}^T(\boldsymbol{u})\boldsymbol{E}\boldsymbol{\varepsilon}(\boldsymbol{u})\, d\Omega.$$

In order to obtain an approximate solution of the weak problem (1), a finite-dimensional counterpart of all these variational forms given above can be built using the Galerkin FEM. We denote $\mathscr{U}_h \subset \mathscr{U}$ and $\mathscr{V}_h \subset \mathscr{V}$ the finite element spaces of continuous functions that are piecewise polynomials of degree $r \geq 1$. The corresponding finite element solution in $\mathscr{U}_h$ is denoted by $\boldsymbol{u}_h$ and satisfies the equation:

$$\int_\Omega \boldsymbol{\varepsilon}^T(\boldsymbol{u}_h)\boldsymbol{E}\boldsymbol{\varepsilon}(\boldsymbol{v})\, d\Omega = \int_\Omega \boldsymbol{b}^T\boldsymbol{v}\, d\Omega + \int_{\Gamma_N} \boldsymbol{t}^T\boldsymbol{v}\, d\Gamma \quad \forall \boldsymbol{v} \in \mathscr{V}_h.$$

Now let us consider the output, which is a linear functional of the solution $\boldsymbol{u}$ defined as $\ell^{\mathcal{O}}(\boldsymbol{u})$, i.e. $\ell^{\mathcal{O}} : (H^1(\Omega))^d \mapsto \mathbb{R}$. Since the output is used in the right hand side of the dual problem defined as follows, it is required that the outputs should depend explicitly on the solution $\boldsymbol{u}$.

In order to derive upper and lower bounds on the output $\ell^{\mathcal{O}}(\boldsymbol{u})$, we introduce the following adjoint or dual problem: find $\boldsymbol{u}^{\mathcal{D}} \in \mathscr{U}$ such that

$$\int_\Omega \boldsymbol{\varepsilon}^T(\boldsymbol{v})\boldsymbol{E}\boldsymbol{\varepsilon}(\boldsymbol{u}^{\mathcal{D}})\, d\Omega = \ell^{\mathcal{O}}(\boldsymbol{v}) \quad \forall \boldsymbol{v} \in \mathscr{V}, \tag{2}$$

and the corresponding finite element approximation, $\boldsymbol{u}_h^{\mathcal{D}} \in \mathscr{U}_h \subset \mathscr{U}$, such that

$$\int_\Omega \boldsymbol{\varepsilon}^T(\boldsymbol{v})\boldsymbol{E}\boldsymbol{\varepsilon}(\boldsymbol{u}_h^{\mathcal{D}})\, d\Omega = \ell^{\mathcal{O}}(\boldsymbol{v}) \quad \forall \boldsymbol{v} \in \mathscr{V}_h. \tag{3}$$

For any displacement $\boldsymbol{u}$ in $\mathscr{U}$, we can write $\boldsymbol{u} = \boldsymbol{u}_D + \boldsymbol{u}^{\mathcal{P}}$ such that $\boldsymbol{u}^{\mathcal{P}} \in \mathscr{V}$ satisfies

$$\int_\Omega \boldsymbol{\varepsilon}^T(\boldsymbol{u}^{\mathcal{P}})\boldsymbol{E}\boldsymbol{\varepsilon}(\boldsymbol{v})\, d\Omega = \int_\Omega \boldsymbol{b}^T\boldsymbol{v}\, d\Omega + \int_{\Gamma_N} \boldsymbol{t}^T\boldsymbol{v}\, d\Gamma - \int_\Omega \boldsymbol{\varepsilon}^T(\boldsymbol{u}_D)\boldsymbol{E}\boldsymbol{\varepsilon}(\boldsymbol{v})\, d\Omega \quad \forall \boldsymbol{v} \in \mathscr{V}_h,$$

and the output

$$\ell^{\mathcal{O}}(\boldsymbol{u}) = \ell^{\mathcal{O}}(\boldsymbol{u}_D) + \ell^{\mathcal{O}}(\boldsymbol{u}^{\mathcal{P}}),$$

therefore computing bounds on output $\ell^{\mathcal{O}}(\boldsymbol{u}^{\mathcal{P}})$ is equivalent to computing bounds on output $\ell^{\mathcal{O}}(\boldsymbol{u})$. Since the dual problem (2) holds for any $\boldsymbol{v}$ in $\mathscr{V}$ and $\boldsymbol{u}^{\mathcal{P}}$ belongs to $\mathscr{V}$, one can write the output $\ell^{\mathcal{O}}(\boldsymbol{u}^{\mathcal{P}})$ as

$$\ell^{\mathcal{O}}(\boldsymbol{u}^{\mathcal{P}}) = \int_\Omega \boldsymbol{\varepsilon}^T(\boldsymbol{u}^{\mathcal{P}})\boldsymbol{E}\boldsymbol{\varepsilon}(\boldsymbol{u}^{\mathcal{D}})\, d\Omega.$$

Using the parallelogram identity, we can also rewrite the above output in the form as follows

$$\ell^{\mathcal{O}}(\boldsymbol{u}^{\mathcal{P}}) = \tfrac{1}{4}\left\|\kappa\boldsymbol{u}^{\mathcal{P}} + \frac{1}{\kappa}\boldsymbol{u}^{\mathcal{D}}\right\|^2 - \tfrac{1}{4}\left\|\kappa\boldsymbol{u}^{\mathcal{P}} - \frac{1}{\kappa}\boldsymbol{u}^{\mathcal{D}}\right\|^2,$$

where $\kappa \in \mathbb{R}$ is a parameter to be optimized to narrow the gap between upper and lower bounds afterwards, and surely $\ell^{\mathcal{O}}(\boldsymbol{u}^{\mathcal{P}})$ satisfies the following inequalities

$$\tfrac{1}{4}\left\|\kappa\boldsymbol{u}^{\mathcal{P}} + \frac{1}{\kappa}\boldsymbol{u}^{\mathcal{D}}\right\|_{LB}^2 - \tfrac{1}{4}\left\|\kappa\boldsymbol{u}^{\mathcal{P}} - \frac{1}{\kappa}\boldsymbol{u}^{\mathcal{D}}\right\|_{UB}^2 \leq \ell^{\mathcal{O}}(\boldsymbol{u}^{\mathcal{P}}) \leq \tfrac{1}{4}\left\|\kappa\boldsymbol{u}^{\mathcal{P}} + \frac{1}{\kappa}\boldsymbol{u}^{\mathcal{D}}\right\|_{UB}^2 - \tfrac{1}{4}\left\|\kappa\boldsymbol{u}^{\mathcal{P}} - \frac{1}{\kappa}\boldsymbol{u}_h^{\mathcal{D}}\right\|_{LB}^2,$$

where the subscripts LB and UB denote the lower and upper bounds respectively, e.g. $\|\cdot\|_{LB} \leq \|\cdot\| \leq \|\cdot\|_{UB}$. We can see these expressions of upper and lower bounds are non-computable, since they depend on the exact solution of both the primal and dual problems. We can use finite elements (displacement method) to compute a lower bound on $\left\|\kappa\boldsymbol{u}^{\mathcal{P}} \pm \frac{1}{\kappa}\boldsymbol{u}^{\mathcal{D}}\right\|$. Since $\|\boldsymbol{u}_h^{\mathcal{P}}\| \leq \|\boldsymbol{u}^{\mathcal{P}}\|$ and $\|\boldsymbol{u}_h^{\mathcal{D}}\| \leq \|\boldsymbol{u}^{\mathcal{D}}\|$, $\left\|\kappa\boldsymbol{u}_h^{\mathcal{P}} \pm \frac{1}{\kappa}\boldsymbol{u}_h^{\mathcal{D}}\right\| \leq \left\|\kappa\boldsymbol{u}^{\mathcal{P}} \pm \frac{1}{\kappa}\boldsymbol{u}^{\mathcal{D}}\right\|$ as the problem is linear, then we can rewrite the bounding formulation as

$$\tfrac{1}{4}\left\|\kappa\boldsymbol{u}_h^{\mathcal{P}} + \frac{1}{\kappa}\boldsymbol{u}_h^{\mathcal{D}}\right\|^2 - \tfrac{1}{4}\left\|\kappa\boldsymbol{u}^{\mathcal{P}} - \frac{1}{\kappa}\boldsymbol{u}^{\mathcal{D}}\right\|_{UB}^2 \leq \ell^{\mathcal{O}}(\boldsymbol{u}^{\mathcal{P}}) \leq \tfrac{1}{4}\left\|\kappa\boldsymbol{u}^{\mathcal{P}} + \frac{1}{\kappa}\boldsymbol{u}^{\mathcal{D}}\right\|_{UB}^2 - \tfrac{1}{4}\left\|\kappa\boldsymbol{u}_h^{\mathcal{P}} - \frac{1}{\kappa}\boldsymbol{u}_h^{\mathcal{D}}\right\|^2. \tag{4}$$

The key ingredient for computing output bounds are finding an upper bound on $\left\|\kappa\boldsymbol{u}^{\mathcal{P}} \pm \frac{1}{\kappa}\boldsymbol{u}^{\mathcal{D}}\right\|^2$, if we can compute upper bound $\left\|\kappa\boldsymbol{u}^{\mathcal{P}} \pm \frac{1}{\kappa}\boldsymbol{u}^{\mathcal{D}}\right\|_{UB}^2$ on $\left\|\kappa\boldsymbol{u}^{\mathcal{P}} \pm \frac{1}{\kappa}\boldsymbol{u}^{\mathcal{D}}\right\|^2$, we can obtain an output bounds according to (4). More details for deriving the above formulations can be found in [8, 9]. We write the expansion of the upper bound as

$$\left\|\kappa\boldsymbol{u}^{\mathcal{P}} \pm \frac{1}{\kappa}\boldsymbol{u}^{\mathcal{D}}\right\|_{UB}^2 \equiv \kappa^2\mathcal{Z}^{\mathcal{P}} + \frac{1}{\kappa^2}\mathcal{Z}^{\mathcal{D}} \pm 2\mathcal{Z}^{\mathcal{I}}, \tag{5}$$

where $\mathcal{Z}^{\mathcal{P}}$ is an upper bound on $\|\boldsymbol{u}^{\mathcal{P}}\|^2$, $\mathcal{Z}^{\mathcal{D}}$ an upper bound on $\|\boldsymbol{u}^{\mathcal{D}}\|^2$, $\mathcal{Z}^{\mathcal{I}}$ a cross inner product with respect to $\mathcal{Z}^{\mathcal{P}}$ and $\mathcal{Z}^{\mathcal{D}}$, whose specific computable forms will be given in next section. The parameter κ is optimized to reduce the bounds gap which is

$$\kappa^2 = \sqrt{\frac{\mathcal{Z}^{\mathcal{D}} - \|\boldsymbol{u}_h^{\mathcal{D}}\|^2}{\mathcal{Z}^{\mathcal{P}} - \|\boldsymbol{u}_h^{\mathcal{P}}\|^2}}. \tag{6}$$

Letting $\boldsymbol{v} = \boldsymbol{u}_h^{\mathcal{P}}$ in equation (3) gives

$$\ell^{\mathcal{O}}(\boldsymbol{u}_h^{\mathcal{P}}) = \int_\Omega \boldsymbol{\varepsilon}^T(\boldsymbol{u}_h^{\mathcal{P}})\boldsymbol{E}\boldsymbol{\varepsilon}(\boldsymbol{u}_h^{\mathcal{D}})\, d\Omega, \tag{7}$$

then with equations (4), (5), (6), and (7) we obtain an upper and lower bounds on $\ell^{\mathcal{O}}(\boldsymbol{u}^{\mathcal{P}})$ in the following compact formulations:

$$\begin{aligned} \ell^{+} &= \tfrac{1}{2}\ell^{\mathcal{O}}(\boldsymbol{u}_h^{\mathcal{P}}) + \tfrac{1}{2}\mathcal{Z}^{\mathcal{I}} + \tfrac{1}{2}\sqrt{\left(\mathcal{Z}^{\mathcal{P}} - \|\boldsymbol{u}_h^{\mathcal{P}}\|^2\right)\left(\mathcal{Z}^{\mathcal{D}} - \|\boldsymbol{u}_h^{\mathcal{D}}\|^2\right)}\,, \\ \ell^{-} &= \tfrac{1}{2}\ell^{\mathcal{O}}(\boldsymbol{u}_h^{\mathcal{P}}) + \tfrac{1}{2}\mathcal{Z}^{\mathcal{I}} - \tfrac{1}{2}\sqrt{\left(\mathcal{Z}^{\mathcal{P}} - \|\boldsymbol{u}_h^{\mathcal{P}}\|^2\right)\left(\mathcal{Z}^{\mathcal{D}} - \|\boldsymbol{u}_h^{\mathcal{D}}\|^2\right)}\,. \end{aligned} \tag{8}$$

3 The smoothed finite element method

Let us partition the computational domain Ω into smoothing subdomains $\bar{\Omega} = \bar{\Omega}_1 \cup \bar{\Omega}_2 \cup ... \cup \bar{\Omega}_N$ with $\Omega_i \cap \Omega_j = \emptyset$ if $i \neq j$, where N is the number of finite element nodes (including the nodes on Γ_D) located in the entire computational domain, and for every node $k = 1, \cdots, N$, the smoothing domain Ω_k is obtained by connecting sequentially the mid-edge point to the centroid of the surrounding triangles of the node as shown in Fig. 1.

Given any strain field $\boldsymbol{\varepsilon}$, the smoothed strain field $\hat{\boldsymbol{\varepsilon}}$ on each smoothing domain Ω_k is obtained by a nodal smoothing operation as

$$\hat{\boldsymbol{\varepsilon}}_k = \int_{\Omega_k} \boldsymbol{\omega}_k(\boldsymbol{x} - \boldsymbol{x}_k)\, \boldsymbol{\varepsilon}\, d\Omega,$$

where $\boldsymbol{\omega}_k(\boldsymbol{x})$ is a diagonal matrix of the smoothing function $\omega_k(\boldsymbol{x})$ that is positive and normalized to unity:

$$\int_{\Omega_k} \omega_k(\boldsymbol{x})\, d\Omega \equiv 1.$$

The smoothed strain $\hat{\boldsymbol{\varepsilon}}_k$ is a constant over the smoothing domain Ω_k. For two-dimensional elasticity problems the diagonal matrix can be chosen to be $\boldsymbol{\omega}_k(\boldsymbol{x}) = \text{diag}\{\omega_k(\boldsymbol{x}), \omega_k(\boldsymbol{x}), \omega_k(\boldsymbol{x})\}$. For simplicity the smoothing function $\omega_k(\boldsymbol{x})$ is taken as

$$\omega_k(\boldsymbol{x} - \boldsymbol{x}_k) = \begin{cases} 1/A_k, & \text{if } \boldsymbol{x} \in \Omega_k \\ 0, & \text{otherwise} \end{cases}$$

where $A_k = \int_{\Omega_k} d\Omega$ is the area of the smoothing domain Ω_k. Therefore, the smoothed strain in the smoothing domain Ω_k will be

$$\hat{\boldsymbol{\varepsilon}}_k = \frac{1}{A_k} \int_{\Omega_k} \boldsymbol{\varepsilon}\, d\Omega. \tag{9}$$

The SFEM is obtained by replacing in the weak form (1) the exact strain field $\boldsymbol{\varepsilon}$ with the nodally smoothed strain field $\hat{\boldsymbol{\varepsilon}}$. The SFEM solution $\hat{\boldsymbol{u}}_h$ is an approximation of the solution, $\boldsymbol{u}$, to the partial differential equation of elasticity. Denote by Φ_i the shape function matrix for node i, for example for two-dimensional problems the shape function matrix

$$\Phi_i(\boldsymbol{x}) = \begin{bmatrix} \phi_i(\boldsymbol{x}) & 0 \\ 0 & \phi_i(\boldsymbol{x}) \end{bmatrix},$$

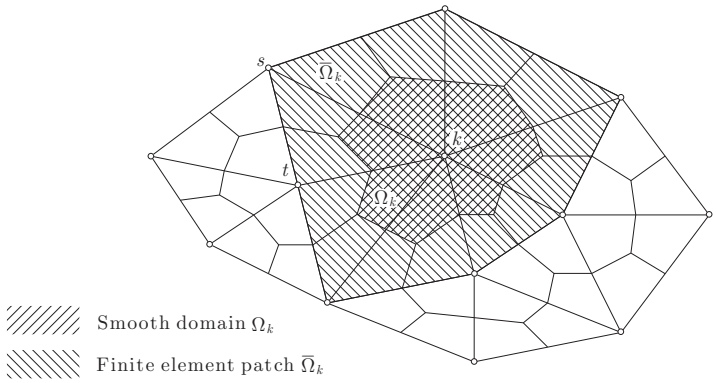

Figure 1: The finite element mesh and the smoothing domain Ω_k.

in which $\phi_i(\boldsymbol{x})$ is the shape function for node i. The SFEM solution is then expressed as

$$\hat{\boldsymbol{u}}_h = \sum_{i=1}^{N} \Phi_i(\boldsymbol{x}) \hat{\boldsymbol{u}}_h^i, \tag{10}$$

where $\hat{\boldsymbol{u}}_h^i = \{\hat{u}_{hx}^i, \hat{u}_{hy}^i\}^T$ is the vector of displacements at node i. Since the strain field is given by the derivatives of displacement, we define the approximate strain obtained from the approximate displacements as $\boldsymbol{\varepsilon}(\hat{\boldsymbol{u}}_h)$, that is

$$\boldsymbol{\varepsilon}(\hat{\boldsymbol{u}}_h) = \sum_{i=1}^{N} \mathcal{D}\Phi_i(\boldsymbol{x}) \hat{\boldsymbol{u}}_h^i. \tag{11}$$

For the two-dimensional elasticity problem

$$\mathcal{D} = \begin{bmatrix} \dfrac{\partial}{\partial x} & 0 \\ 0 & \dfrac{\partial}{\partial y} \\ \dfrac{\partial}{\partial y} & \dfrac{\partial}{\partial x} \end{bmatrix},$$

and so according to (9) by replacing $\boldsymbol{\varepsilon}$ with $\boldsymbol{\varepsilon}(\hat{\boldsymbol{u}}_h)$ we obtain the smoothed strain $\hat{\boldsymbol{\varepsilon}}_k$,

$$\hat{\boldsymbol{\varepsilon}}_k(\hat{\boldsymbol{u}}_h) = \frac{1}{A_k} \int_{\Omega_k} \boldsymbol{\varepsilon}(\hat{\boldsymbol{u}}_h)\, d\Omega, \tag{12}$$

and, more specifically,

$$\begin{aligned}\hat{\boldsymbol{\varepsilon}}_k(\hat{\boldsymbol{u}}_h) &= \frac{1}{A_k}\sum_{i=1}^{N}\left(\int_{\Omega_k}\mathcal{D}\Phi_i(\boldsymbol{x})\,d\Omega\right)\hat{\boldsymbol{u}}_h^i \\ &= \frac{1}{A_k}\sum_{i\in\mathcal{N}_k}\left(\int_{\Omega_k}\mathcal{D}\Phi_i(\boldsymbol{x})\,d\Omega\right)\hat{\boldsymbol{u}}_h^i \\ &= \frac{1}{A_k}\sum_{i\in\mathcal{N}_k}\hat{\mathcal{B}}_k^i\hat{\boldsymbol{u}}_h^i,\end{aligned}$$

where $\mathcal{N}_k$ includes all nodes in the patch $\bar{\Omega}_k$ that is formed by the elements sharing node k, and

$$\hat{\mathcal{B}}_k^i = \int_{\Omega_k}\mathcal{D}\Phi_i(\boldsymbol{x})\,d\Omega.$$

In the next step we will derive the stiffness matrix. The strain energy in the smoothing domain Ω_k is

$$\begin{aligned}\int_{\Omega_k}\hat{\boldsymbol{\varepsilon}}_k^T(\hat{\boldsymbol{u}}_h)\boldsymbol{E}\hat{\boldsymbol{\varepsilon}}_k(\hat{\boldsymbol{u}}_h)\,d\Omega &= A_k\hat{\boldsymbol{\varepsilon}}_k^T(\hat{\boldsymbol{u}}_h)\boldsymbol{E}\hat{\boldsymbol{\varepsilon}}_k(\hat{\boldsymbol{u}}_h) \\ &= \frac{1}{A_k}\sum_{i\in\mathcal{N}_k}\sum_{j\in\mathcal{N}_k}\hat{\boldsymbol{u}}_h^{iT}(\hat{\boldsymbol{u}}_h)\hat{\mathcal{B}}_k^{iT}\boldsymbol{E}\hat{\mathcal{B}}_k^j\hat{\boldsymbol{u}}_h^j.\end{aligned}$$

Therefore, the local stiffness matrix associated with node k is obtained as

$$\hat{\boldsymbol{K}}_{ij(k)} = \frac{1}{A_k}\hat{\mathcal{B}}_k^{iT}\boldsymbol{E}\hat{\mathcal{B}}_k^j, \tag{13}$$

and the global stiffness matrix for SFEM will be

$$\hat{\boldsymbol{K}}_{ij} = \sum_{k=1}^{N}\hat{\boldsymbol{K}}_{ij(k)}.$$

The entries (in sub-vectors of nodal forces) of the force vector $\hat{\boldsymbol{f}}$ in the right hand side of the algebraic system can be simply expressed as

$$\hat{\boldsymbol{f}}_i = \sum_{k\in\mathcal{N}_k}\hat{\boldsymbol{f}}_{i(k)}. \tag{14}$$

The above integration is also performed by a summation of integrals over smoothing domains; hence, $\hat{\boldsymbol{f}}_i$ is an assembly of nodal force vectors at the surrounding nodes of node k,

$$\hat{\boldsymbol{f}}_{i(k)} = \int_{\Omega_{(k)}}\Phi_i(\boldsymbol{x})\boldsymbol{b}\,d\Omega + \int_{\Gamma_{t(k)}}\Phi_i(\boldsymbol{x})\boldsymbol{t}\,d\Gamma.$$

Note that the force vector obtained in SFEM is the same as the one in FEM, if the same order shape functions is used. This simplifies the implementation of SFEM. In the Appendix, we give the implementation of SFEM with linear triangle elements in detail.

In the sequel we will give some properties of SFEM. Lemma 1 gives the orthogonality property for SFEM [15].

Lemma 1 *For any compatible strain field $\boldsymbol{\varepsilon}(\hat{\boldsymbol{u}}_h) = \mathcal{D}\hat{\boldsymbol{u}}_h$ obtained by (11) on a finite element mesh $\mathcal{T}_h$, and the smoothed strain $\hat{\boldsymbol{\varepsilon}}(\hat{\boldsymbol{u}}_h)$ obtained by (12) on the same mesh, we have the orthogonality property:*

$$\int_\Omega \boldsymbol{\varepsilon}^T(\hat{\boldsymbol{u}}_h)\boldsymbol{E}\hat{\boldsymbol{\varepsilon}}(\hat{\boldsymbol{u}}_h)\,d\Omega = \int_\Omega \hat{\boldsymbol{\varepsilon}}^T(\hat{\boldsymbol{u}}_h)\boldsymbol{E}\hat{\boldsymbol{\varepsilon}}(\hat{\boldsymbol{u}}_h)\,d\Omega. \tag{15}$$

Proof We note that $\hat{\boldsymbol{\varepsilon}}(\hat{\boldsymbol{u}}_h)$ is a piecewise constant function over the whole domain. Equation (15) can be easily proven by relying on equation (12) and the fact that $\boldsymbol{E}\hat{\boldsymbol{\varepsilon}}_k(\hat{\boldsymbol{u}}_h)$ is constant over Ω_k, so that the left hand side is a sum of the cross inner product

$$\begin{aligned}
\int_\Omega \boldsymbol{\varepsilon}^T(\hat{\boldsymbol{u}}_h)\boldsymbol{E}\hat{\boldsymbol{\varepsilon}}(\hat{\boldsymbol{u}}_h)\,d\Omega &= \sum_{k=1}^{N}\int_{\Omega_k} \boldsymbol{\varepsilon}^T(\hat{\boldsymbol{u}}_h)\boldsymbol{E}\hat{\boldsymbol{\varepsilon}}_k(\hat{\boldsymbol{u}}_h)\,d\Omega \\
&= \sum_{k=1}^{N}\left(\int_{\Omega_k} \boldsymbol{\varepsilon}^T(\hat{\boldsymbol{u}}_h)\,d\Omega\right)\boldsymbol{E}\hat{\boldsymbol{\varepsilon}}_k(\hat{\boldsymbol{u}}_h) \\
&= \sum_{k=1}^{N} A_k\hat{\boldsymbol{\varepsilon}}_k^T(\hat{\boldsymbol{u}}_h)\boldsymbol{E}\hat{\boldsymbol{\varepsilon}}_k(\hat{\boldsymbol{u}}_h) \\
&= \int_\Omega \hat{\boldsymbol{\varepsilon}}^T(\hat{\boldsymbol{u}}_h)\boldsymbol{E}\hat{\boldsymbol{\varepsilon}}(\hat{\boldsymbol{u}}_h)\,d\Omega.
\end{aligned} \tag{16}$$

□

With the above orthogonality we can obtain other properties of SFEM.

Remark 1
The strain energy of the SFEM solution computed with the smoothed strain in $\mathscr{V}_h$ always bounds the strain energy obtained with the compatible strain in $\mathscr{V}_h$ from below:

$$\int_\Omega \hat{\boldsymbol{\varepsilon}}^T(\hat{\boldsymbol{u}}_h)\boldsymbol{E}\hat{\boldsymbol{\varepsilon}}(\hat{\boldsymbol{u}}_h)\,d\Omega \le \int_\Omega \boldsymbol{\varepsilon}^T(\hat{\boldsymbol{u}}_h)\boldsymbol{E}\boldsymbol{\varepsilon}(\hat{\boldsymbol{u}}_h)\,d\Omega. \tag{17}$$

Proof We have

$$\begin{aligned}
0 &\leq \int_\Omega \left(\boldsymbol{\varepsilon}^T(\hat{\boldsymbol{u}}_h) - \hat{\boldsymbol{\varepsilon}}^T(\hat{\boldsymbol{u}}_h)\right) \boldsymbol{E}\left(\boldsymbol{\varepsilon}(\hat{\boldsymbol{u}}_h) - \hat{\boldsymbol{\varepsilon}}(\hat{\boldsymbol{u}}_h)\right)\, d\Omega \\
&= \int_\Omega \boldsymbol{\varepsilon}^T(\hat{\boldsymbol{u}}_h)\boldsymbol{E}\boldsymbol{\varepsilon}(\hat{\boldsymbol{u}}_h)\, d\Omega + \int_\Omega \hat{\boldsymbol{\varepsilon}}^T(\hat{\boldsymbol{u}}_h)\boldsymbol{E}\hat{\boldsymbol{\varepsilon}}(\hat{\boldsymbol{u}}_h)\, d\Omega - 2\int_\Omega \boldsymbol{\varepsilon}^T(\hat{\boldsymbol{u}}_h)\boldsymbol{E}\hat{\boldsymbol{\varepsilon}}(\hat{\boldsymbol{u}}_h)\, d\Omega \\
&= \int_\Omega \boldsymbol{\varepsilon}^T(\hat{\boldsymbol{u}}_h)\boldsymbol{E}\boldsymbol{\varepsilon}(\hat{\boldsymbol{u}}_h)\, d\Omega - \int_\Omega \hat{\boldsymbol{\varepsilon}}^T(\hat{\boldsymbol{u}}_h)\boldsymbol{E}\hat{\boldsymbol{\varepsilon}}(\hat{\boldsymbol{u}}_h)\, d\Omega.
\end{aligned}$$

□

Remark 2
The strain energy of the FEM solution computed with the smoothed strain in $\mathscr{V}_h$ always bounds the strain energy obtained with the compatible strain in $\mathscr{V}_h$ from below:

$$\int_\Omega \hat{\boldsymbol{\varepsilon}}^T(\boldsymbol{u}_h)\boldsymbol{E}\hat{\boldsymbol{\varepsilon}}(\boldsymbol{u}_h)\, d\Omega \leq \int_\Omega \boldsymbol{\varepsilon}^T(\boldsymbol{u}_h)\boldsymbol{E}\boldsymbol{\varepsilon}(\boldsymbol{u}_h)\, d\Omega. \tag{18}$$

Proof Since the inequality of Remark 1 holds for any displacement on mesh $\mathcal{T}_h$, we can replace $\hat{\boldsymbol{u}}_h$ with $\boldsymbol{u}_h$, i.e. the finite element solution expressed with the same form as (10),

$$\boldsymbol{u}_h = \sum_{i=1}^{N} \Phi_i(\boldsymbol{x})\boldsymbol{u}_h^i,$$

and obtain the lower bounds on the strain energy computed with FEM,

$$\int_\Omega \hat{\boldsymbol{\varepsilon}}^T(\boldsymbol{u}_h)\boldsymbol{E}\hat{\boldsymbol{\varepsilon}}(\boldsymbol{u}_h)\, d\Omega \leq \int_\Omega \boldsymbol{\varepsilon}^T(\boldsymbol{u}_h)\boldsymbol{E}\boldsymbol{\varepsilon}(\boldsymbol{u}_h)\, d\Omega.$$

□

Theorem 1 *The smoothed strain energy of SFEM bounds the strain energy of FEM from above:*

$$\int_\Omega \boldsymbol{\varepsilon}^T(\boldsymbol{u}_h)\boldsymbol{E}\boldsymbol{\varepsilon}(\boldsymbol{u}_h)\, d\Omega \leq \int_\Omega \hat{\boldsymbol{\varepsilon}}^T(\hat{\boldsymbol{u}}_h)\boldsymbol{E}\hat{\boldsymbol{\varepsilon}}(\hat{\boldsymbol{u}}_h)\, d\Omega. \tag{19}$$

Proof The weak form for FEM is

$$\int_\Omega \boldsymbol{\varepsilon}^T(\boldsymbol{u}_h)\boldsymbol{E}\boldsymbol{\varepsilon}(\boldsymbol{v})\, d\Omega = \int_\Omega \boldsymbol{b}^T\boldsymbol{v}\, d\Omega + \int_{\Gamma_N} \boldsymbol{t}^T\boldsymbol{v}\, d\Gamma \quad \forall \boldsymbol{v} \in \mathscr{V}_h,$$

after choosing $\boldsymbol{v} = \boldsymbol{u}_h$ into the above equation, we have

$$\int_\Omega \boldsymbol{\varepsilon}^T(\boldsymbol{u}_h)\boldsymbol{E}\boldsymbol{\varepsilon}(\boldsymbol{u}_h)\, d\Omega = \int_\Omega \boldsymbol{b}^T\boldsymbol{u}_h\, d\Omega + \int_{\Gamma_N} \boldsymbol{t}^T\boldsymbol{u}_h\, d\Gamma.$$

Both FEM and SFEM have the same right hand side as (14) in the discrete form when the same shape function is used on mesh $\mathcal{T}_h$, then with the finite element solution $\boldsymbol{u}_h$ as the test function to SFEM we get

$$\int_\Omega \hat{\boldsymbol{\varepsilon}}^T(\hat{\boldsymbol{u}}_h)\boldsymbol{E}\hat{\boldsymbol{\varepsilon}}(\boldsymbol{u}_h)\,d\Omega = \int_\Omega \boldsymbol{b}^T\boldsymbol{u}_h\,d\Omega + \int_{\Gamma_N} \boldsymbol{t}^T\boldsymbol{u}_h\,d\Gamma,$$

By comparing the above two equations, we have

$$\int_\Omega \boldsymbol{\varepsilon}^T(\boldsymbol{u}_h)\boldsymbol{E}\boldsymbol{\varepsilon}(\boldsymbol{u}_h)\,d\Omega = \int_\Omega \hat{\boldsymbol{\varepsilon}}^T(\hat{\boldsymbol{u}}_h)\boldsymbol{E}\hat{\boldsymbol{\varepsilon}}(\boldsymbol{u}_h)\,d\Omega.$$

In a similar way used for the derivation of equation (16), we can omit the hat of $\hat{\boldsymbol{\varepsilon}}(\boldsymbol{u}_h)$ on the right hand side of the above equation, and obtain

$$\int_\Omega \hat{\boldsymbol{\varepsilon}}^T(\hat{\boldsymbol{u}}_h)\boldsymbol{E}\hat{\boldsymbol{\varepsilon}}(\boldsymbol{u}_h)\,d\Omega = \int_\Omega \hat{\boldsymbol{\varepsilon}}^T(\hat{\boldsymbol{u}}_h)\boldsymbol{E}\boldsymbol{\varepsilon}(\boldsymbol{u}_h)\,d\Omega,$$

then, from the two equations above, we get

$$\int_\Omega \boldsymbol{\varepsilon}^T(\boldsymbol{u}_h)\boldsymbol{E}\boldsymbol{\varepsilon}(\boldsymbol{u}_h)\,d\Omega = \int_\Omega \hat{\boldsymbol{\varepsilon}}^T(\hat{\boldsymbol{u}}_h)\boldsymbol{E}\boldsymbol{\varepsilon}(\boldsymbol{u}_h)\,d\Omega. \tag{20}$$

With the following derivation

$$\begin{aligned}
0 &\le \int_\Omega \left(\hat{\boldsymbol{\varepsilon}}^T(\hat{\boldsymbol{u}}_h) - \boldsymbol{\varepsilon}^T(\boldsymbol{u}_h)\right)\boldsymbol{E}\left(\hat{\boldsymbol{\varepsilon}}(\hat{\boldsymbol{u}}_h) - \boldsymbol{\varepsilon}(\boldsymbol{u}_h)\right)\,d\Omega \\
&= \int_\Omega \hat{\boldsymbol{\varepsilon}}^T(\hat{\boldsymbol{u}}_h)\boldsymbol{E}\hat{\boldsymbol{\varepsilon}}(\hat{\boldsymbol{u}}_h)\,d\Omega + \int_\Omega \boldsymbol{\varepsilon}^T(\boldsymbol{u}_h)\boldsymbol{E}\boldsymbol{\varepsilon}(\boldsymbol{u}_h)\,d\Omega - 2\int_\Omega \hat{\boldsymbol{\varepsilon}}^T(\hat{\boldsymbol{u}}_h)\boldsymbol{E}\boldsymbol{\varepsilon}(\boldsymbol{u}_h)\,d\Omega \\
&= \int_\Omega \hat{\boldsymbol{\varepsilon}}^T(\hat{\boldsymbol{u}}_h)\boldsymbol{E}\hat{\boldsymbol{\varepsilon}}(\hat{\boldsymbol{u}}_h)\,d\Omega - \int_\Omega \boldsymbol{\varepsilon}^T(\boldsymbol{u}_h)\boldsymbol{E}\boldsymbol{\varepsilon}(\boldsymbol{u}_h)\,d\Omega,
\end{aligned}$$

and remarking that the last step in the above equation is obtained according to equation (20), we obtain an upper bound on the energy norm of the solution by FEM as

$$\int_\Omega \boldsymbol{\varepsilon}^T(\boldsymbol{u}_h)\boldsymbol{E}\boldsymbol{\varepsilon}(\boldsymbol{u}_h)\,d\Omega \le \int_\Omega \hat{\boldsymbol{\varepsilon}}^T(\hat{\boldsymbol{u}}_h)\boldsymbol{E}\hat{\boldsymbol{\varepsilon}}(\hat{\boldsymbol{u}}_h)\,d\Omega.$$

□

With equations (17), (18), and (19) we obtain a sequence of inequalities for the strain energies computed with the strains obtained with both FEM and SFEM. References [14, 15] provide the same inequality (19) and proved that the strain energy computed with SFEM is also an upper bound on the exact strain energy, but only under the hypothesis that shape functions exist for exact solutions. Many numerical examples show that SFEM does give upper bounds on the true strain energy, except for some cases where the meshes are too coarse.

Let us set

$$\mathcal{Z}^{\mathcal{P}} = \int_{\Omega} \hat{\boldsymbol{\varepsilon}}^T(\hat{\boldsymbol{u}}_h)\boldsymbol{E}\hat{\boldsymbol{\varepsilon}}(\hat{\boldsymbol{u}}_h)\, d\Omega;$$

$$\mathcal{Z}^{\mathcal{D}} = \int_{\Omega} \hat{\boldsymbol{\varepsilon}}^T(\hat{\boldsymbol{u}}_h^{\mathcal{D}})\boldsymbol{E}\hat{\boldsymbol{\varepsilon}}(\hat{\boldsymbol{u}}_h^{\mathcal{D}})\, d\Omega;$$

and

$$\mathcal{Z}^{\mathcal{I}} = \int_{\Omega} \hat{\boldsymbol{\varepsilon}}^T(\hat{\boldsymbol{u}}_h)\boldsymbol{E}\hat{\boldsymbol{\varepsilon}}(\hat{\boldsymbol{u}}_h^{\mathcal{D}})\, d\Omega.$$

Now we have the final formulations for the quantities appearing in (8) that are needed to compute upper and lower bounds on linear outputs by SFEM.

4 Numerical examples

We illustrate the effectivity of the proposed method on two numerical examples. Linear triangle finite element approximations are used for both primal and dual problems. Uniform mesh refinement is used in all examples to illustrate the bounding property with respect to the mesh size. Since the two examples satisfy homogeneous essential boundary conditions, $\boldsymbol{u}^{\mathcal{P}}$ is exactly $\boldsymbol{u}$ in the previous equations, so we will omit the superscript $\mathcal{P}$ in the equations of this section.

The first example is a square elastic body with two rectangular holes, under the assumption that the body is in plane stress state as shown in Fig. 2. A uniformly distributed force, $p = 1$, is applied on the left and right sides of the body. The non-dimensionalized Young modulus is 1.0 and Poisson ratio is 0.3. Since the geometry and load conditions in this problem are symmetric with respect to both the x- and y-axes, we only use a quarter of the body for the finite element model. Two outputs are considered in this example. The first one

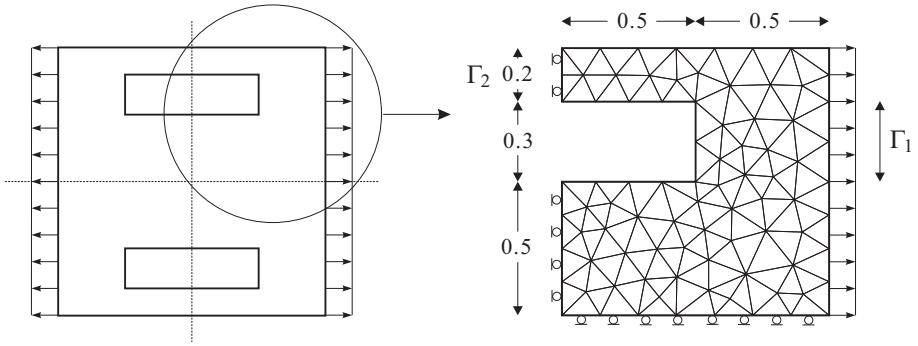

Figure 2: An elasticity problem with symmetric geometry and load condition, a quarter of the structure is used for the finite element modeling. The finite element mesh shown in the right figure is the initial mesh with 132 elements.

is the average normal displacement over the boundary Γ_1,

$$\ell_1^{\mathcal{O}}(\boldsymbol{u}) = \int_{\Gamma_1} \boldsymbol{u}^T \boldsymbol{n} \mathrm{d}\Gamma,$$

in which $\boldsymbol{n}$ is the unit outward normal to the boundary; the second one is the reaction force on boundary Γ_2,

$$\ell_2^{\mathcal{O}}(\boldsymbol{u}) = \int_{\Gamma_2} \boldsymbol{n}^T \left(\boldsymbol{N}\boldsymbol{\sigma}(\boldsymbol{u})\right) \mathrm{d}\Gamma,$$

where

$$\boldsymbol{N} = \begin{bmatrix} n_1 & 0 & n_2 \\ 0 & n_2 & n_1 \end{bmatrix},$$

and n_1 and n_2 are the components of $\boldsymbol{n}$. The initial (coarse) mesh with respect to mesh size H is plotted in Fig. 2. The uniformly refined meshes are based on mesh sizes $H/2$, $H/4$, $H/8$, and $H/16$ respectively. The results for $\ell_1^{\mathcal{O}}(\boldsymbol{u})$ and $\ell_2^{\mathcal{O}}(\boldsymbol{u})$ including the outputs calculated by FEM and SFEM, the upper and lower bounds, and the average of the upper and lower bounds are plotted in Fig. 3. From equation (8) the average of bounds is actually the average of the outputs by FEM and SFEM, that is $\frac{1}{2}(\ell^{\mathcal{O}}(\boldsymbol{u}_h) + \mathcal{Z}^{\mathcal{I}}) = \frac{1}{2}(\ell^{\mathcal{O}}(\boldsymbol{u}_h) + \ell^{\mathcal{O}}(\hat{\boldsymbol{u}}_h))$. We also plot the strain energies computed by FEM and SFEM in both primal and dual problems for the two outputs in Figs. 4-5. We will analyze the effectivity of the bounds by a measure given at the end of this section.

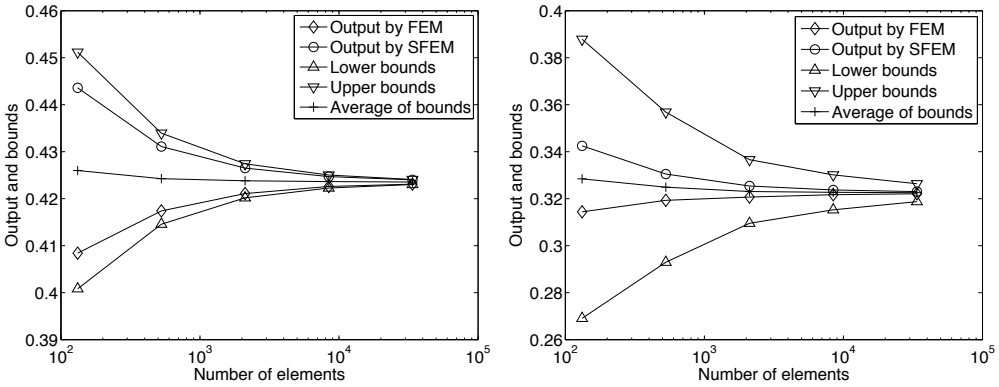

Figure 3: The upper and lower bounds on the displacement output $\ell_1^{\mathcal{O}}(\boldsymbol{u})$ (left) and the reaction output $\ell_2^{\mathcal{O}}(\boldsymbol{u})$ (right).

The second example is a plate with two edge cracks subject to a uniformly distributed tensile stress, as shown in Fig. 6. The plate is assumed to be in plane strain. The value of the tensile force acting on the two ends of the plate is $p = 1$ and the dimension of the crack is $a = 5$. The non-dimensional Young modulus is 1.0 and Poisson ratio is 0.3. The third output $\ell_3^{\mathcal{O}}(\boldsymbol{u})$ we consider is

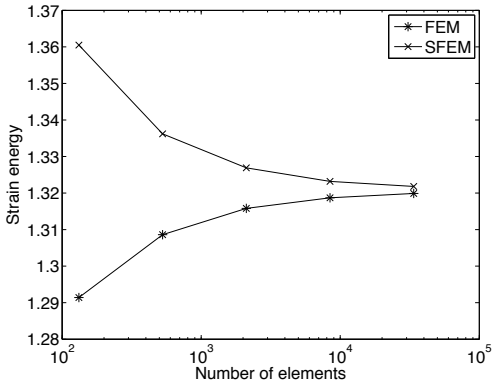

Figure 4: The strain energies computed by FEM and SFEM in the primal problems for the first two outputs.

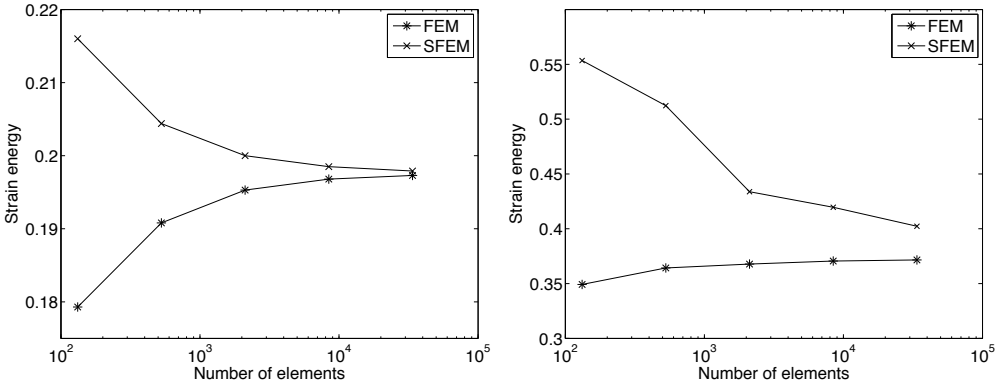

Figure 5: The strain energies computed by FEM and SFEM in the dual problems for the displacement output $\ell_1^{\mathcal{O}}(\boldsymbol{u})$ (left) and the reaction output $\ell_2^{\mathcal{O}}(\boldsymbol{u})$ (right).

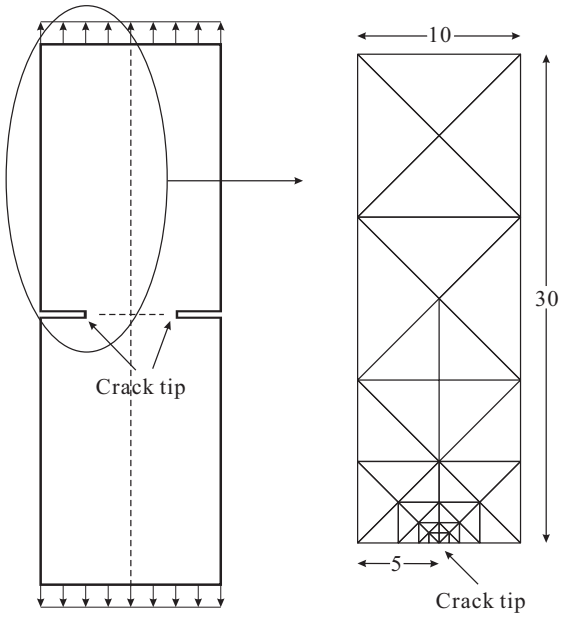

Figure 6: A double edge-cracked elastic plate subject to a uniform tensile stress: just a quarter of the structure is used for the finite element modeling. The finite element mesh shown in the right figure is the initial mesh with 41 elements.

the so-called J-integral, which is defined in the domain integral form as

$$\ell_3^{\mathcal{O}}(\boldsymbol{u}) = \tfrac{1}{2}\int_{\Omega_\chi} \boldsymbol{u}_{\boldsymbol{x}}^T \left[\boldsymbol{Q} - \frac{\partial \chi}{\partial x}\tilde{\boldsymbol{D}}\right] \boldsymbol{u}_{\boldsymbol{x}}\, d\Omega, \tag{21}$$

where the integration domain Ω_χ contains the crack tip,

$$\boldsymbol{u}_{\boldsymbol{x}} = \left\{\frac{\partial u_x}{\partial x}, \frac{\partial u_y}{\partial x}, \frac{\partial u_x}{\partial y}, \frac{\partial u_y}{\partial y}\right\}^T,$$

χ is the weight function equal to one at the crack tip and vanishing on the boundary of Ω_χ, $\boldsymbol{Q}$ and $\tilde{\boldsymbol{D}}$ are matrices containing the elastic parameters and the weight function χ, refer to the appendix in [19]. From equation (21) we see that J-integral is a quadratic function of the displacement, to express the following equations clearly we use $J(\boldsymbol{u}, \boldsymbol{u})$ to express $\ell_3^{\mathcal{O}}(\boldsymbol{u})$, so that we have

$$\begin{aligned} \ell_3^{\mathcal{O}}(\boldsymbol{u}) - \ell_3^{\mathcal{O}}(\boldsymbol{u}_h) &= J(\boldsymbol{u}, \boldsymbol{u}) - J(\boldsymbol{u}_h, \boldsymbol{u}_h) \\ &= J(\boldsymbol{u} - \boldsymbol{u}_h, \boldsymbol{u} - \boldsymbol{u}_h) + 2J(\boldsymbol{u} - \boldsymbol{u}_h, \boldsymbol{u}_h). \end{aligned} \tag{22}$$

In [19] it was found that

$$\begin{aligned} J(\boldsymbol{u} - \boldsymbol{u}_h, \boldsymbol{u} - \boldsymbol{u}_h) &\le \eta_\chi \|\boldsymbol{u} - \boldsymbol{u}_h\|^2 \\ &= \eta_\chi \left(\|\boldsymbol{u}\|^2 - \|\boldsymbol{u}_h\|^2\right) \\ &\le \eta_\chi \left(\|\boldsymbol{u}_h^{\mathcal{D}}\|^2 - \|\boldsymbol{u}_h\|^2\right), \end{aligned} \tag{23}$$

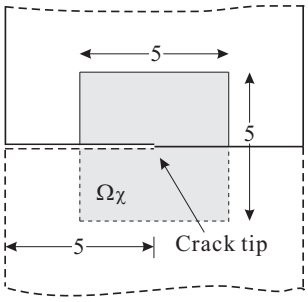

Figure 7: A 5× 5 integral domain Ω_χ is arranged for evaluation of the J-integral.

where η_χ is a computable quantity related to elasticity coefficients and to χ. For the second term in equation (22),

$$J(\boldsymbol{u}-\boldsymbol{u}_h,\boldsymbol{u}_h)=J(\boldsymbol{u},\boldsymbol{u}_h)-J(\boldsymbol{u}_h,\boldsymbol{u}_h), \tag{24}$$

we note $J(\boldsymbol{u},\boldsymbol{u}_h)$ is a linear function of $\boldsymbol{u}$, thus with bounding formulations for the linear output (8), we can compute the upper and lower bounds on $J(\boldsymbol{u},\boldsymbol{u}_h)$, that is

$$\ell^- \le J(\boldsymbol{u},\boldsymbol{u}_h) \le \ell^+ .$$

Let $Q=\eta\left(\|\boldsymbol{u}_h^{\mathcal{D}}\|^2-\|\boldsymbol{u}_h\|^2\right)$ in equation (23), and consider the equations (22), (23), (24) and (8). The upper and lower bounds formulations for the J-integral are summarized as follows:

$$\begin{aligned} J^+ &= \mathcal{Z}^{\mathcal{I}}+Q+\sqrt{(\mathcal{Z}-\|\boldsymbol{u}_h\|^2)\left(\mathcal{Z}^{\mathcal{D}}-\|\boldsymbol{u}_h^{\mathcal{D}}\|^2\right)}\,,\\ J^- &= \mathcal{Z}^{\mathcal{I}}-Q-\sqrt{(\mathcal{Z}-\|\boldsymbol{u}_h\|^2)\left(\mathcal{Z}^{\mathcal{D}}-\|\boldsymbol{u}_h^{\mathcal{D}}\|^2\right)}\,. \end{aligned} \tag{25}$$

In this example, due to the symmetry of the problem, we only use one quarter of the plate for the finite element modeling. We use a 5 by 5 square area surrounding the crack tip as the support, Ω_χ, of the weighting function χ, see Fig. 7. We should note that the J-integral gets a contribution from the entire half plate, but we only use a quarter of the plate for the finite element model, so we need to multiply the outputs computed by this finite element model by two, including the J-integral and all terms on the right hand side of equation (25). There is no such issue for the outputs in the previous example. The bounding results computed are plotted in Fig. 8, where the formulation of average of the bounds is different from that of the first two linear outputs, from (25) we can see the average is $\mathcal{Z}^{\mathcal{I}}$, that is $\mathcal{Z}^{\mathcal{I}}=\ell^{\mathcal{O}}(\hat{\boldsymbol{u}}_h)=J(\hat{\boldsymbol{u}}_h,\boldsymbol{u}_h)$. The strain energies computed by FEM and SFEM in the primal and dual problems are plotted in Fig. 9.

We introduce the relative half bound gap given in [9]

$$\rho_G=\tfrac{1}{2}\frac{\ell^+-\ell^-}{\ell(\boldsymbol{u})}$$

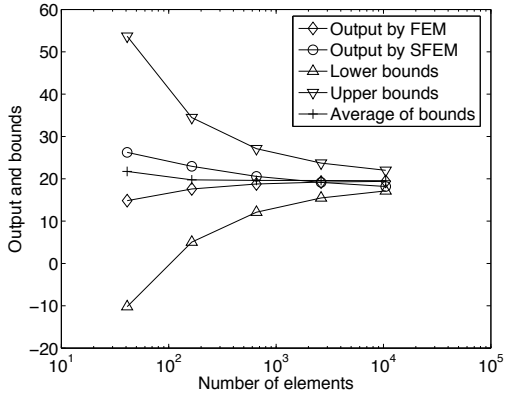

Figure 8: The upper and lower bounds on the J-integral $\ell_3^{\mathcal{O}}(\boldsymbol{u})$.

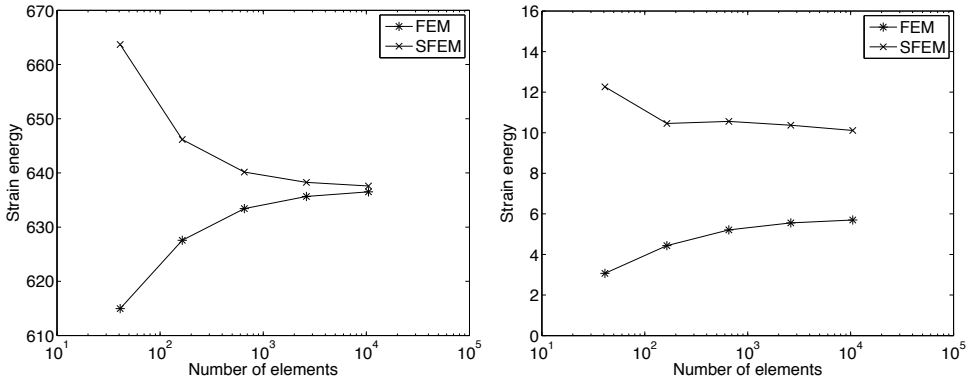

Figure 9: Strain energies computed by FEM and SFEM in the primal problem (left) and the dual problem (right) for the J-integral.

as a measure of the accuracy of the bounds. It is certainly an upper bound on the relative error between the average of the bounds and the exact output $\ell(\boldsymbol{u})$. Since the exact output $\ell(\boldsymbol{u})$ is not known for the examples, we use the average of the bounds calculated with a finer mesh of mesh size $H/16$ instead. Thus a computable measure of the accuracy of the bounds is given by

$$\rho_G = \frac{\ell^+ - \ell^-}{\ell^{*+} + \ell^{*-}},$$

where ℓ^{*+} and ℓ^{*-} are the upper and lower bounds calculated in the mesh with mesh size $H/16$. Fig. 10 shows the convergence results of ρ_G for the three outputs. The convergence rates do not attain the optimal converge rate of 1, because there are singularities (corners and crack tip) in both the two examples. The convergence rate for the displacement output, 0.7, is the biggest, and the relative bound gap is the smallest. The convergence rates for the stress output and the J-integral are 0.5 and 0.46, respectively. The convergence rate for the J-integral is the smallest, because the approximate solutions are dominated by a singularity caused by the crack, which affects the convergence rate much more than the effect caused by corners in the first example. The relative half bound gap for the J-integral is the largest in the three outputs, the main reason being that the difference between the strain energies computed by FEM and SFEM in the dual problem is very large, see the left figure in Fig. 9. The exact strain energy of the dual problem is about 6, but the strain energy computed by SFEM has trouble converging to this value and only provides an upper bound. This is an issue that sometimes arises with SFEM, although it does not happen often. The strain energies computed by SFEM in the primal problem for the J-integral and in both primal and dual problems for other outputs in the first example are very effective.

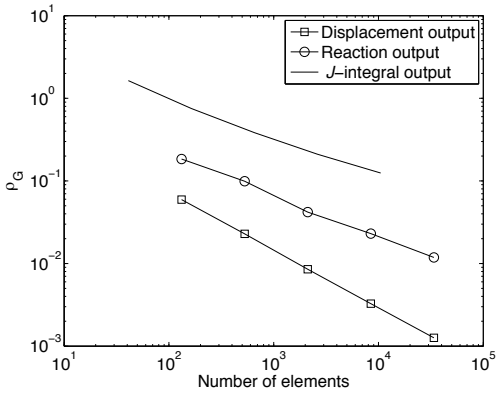

Figure 10: Bounds convergence for the three outputs.

5 Conclusions and discussion

We have examined SFEM with linear triangle elements and extended it to compute upper and lower bounds on general linear outputs of displacements in elasticity. In the examples we have considered, SFEM behaves like an equilibrium method and the strain energy converges to the true strain energy from above. We also find that in some cases the energy norm of the solution by SFEM does not reach the exact strain energy, as shown in the right side of figure Fig. 9, but can be used as an upper bound indicator. However, in most cases SFEM really gives a convergent upper bound on the strain energy and, consequently, also gives convergent upper and lower bounds on general linear outputs. One of the most important advantages of bounds computation by SFEM is that they are very easy to implement, as this simply requires a modification of a few lines of our underlying finite element code to implement SFEM. This is an advantage over the equilibrium method to obtain upper bounds. We also note that many a posteriori error estimates proposed in literature are an order of magnitude more expensive to compute than the finite element solution. In contrast, the computation of upper bounds using SFEM is only about as expensive as solving the regular finite element problem. Further research will be on solving the convergence problem of SFEM, and extending it to solve inelasticity problems as done by Ledevèze and his coworkers [20, 21].

Acknowledgements

This work was performed while the first author was visiting the Chair of Modelling and Scientific Computing (CMCS), Institute of Analysis and Scientific Computing (IACS), École Polytechnique Féderale de Lausanne (EPFL), and was supported by the National Natural Science Foundation of China under grant number 10872146.

Appendix

For two-dimensional elasticity problems, the relation between displacement, $\boldsymbol{u} = \{u_x, u_y\}^T$, and strain, $\boldsymbol{\varepsilon}(\boldsymbol{u})$, is $\boldsymbol{\varepsilon}(\boldsymbol{u}) = \mathcal{D}\boldsymbol{u}$,

$$\boldsymbol{\varepsilon}(\boldsymbol{u}) \equiv \left\{ \begin{array}{c} \dfrac{\partial u_x}{\partial x} \\ \dfrac{\partial u_y}{\partial y} \\ \dfrac{\partial u_y}{\partial x} + \dfrac{\partial u_x}{\partial y} \end{array} \right\} = \left\{ \begin{array}{c} \varepsilon_{11}(\boldsymbol{u}) \\ \varepsilon_{22}(\boldsymbol{u}) \\ 2\varepsilon_{12}(\boldsymbol{u}) \end{array} \right\}, \tag{26}$$

and the corresponding stress according to $\boldsymbol{\sigma} = \boldsymbol{E}\boldsymbol{\varepsilon}(\boldsymbol{u})$ is specifically expressed as

$$\boldsymbol{\sigma} \equiv \begin{Bmatrix} \sigma_{11} \\ \sigma_{22} \\ \sigma_{12} \end{Bmatrix} = \begin{bmatrix} \lambda+2\mu & \lambda & 0 \\ \lambda & \lambda+2\mu & 0 \\ 0 & 0 & \mu \end{bmatrix} \begin{Bmatrix} \varepsilon_{11}(\boldsymbol{u}) \\ \varepsilon_{22}(\boldsymbol{u}) \\ 2\varepsilon_{12}(\boldsymbol{u}) \end{Bmatrix},$$

where λ and μ are Lame's constants, $\mu = \frac{E}{2(1+\nu)}$, and $\lambda = \frac{E\nu}{(1+\nu)(1-2\nu)}$ for plane strain problem, $\lambda = \frac{E\nu}{1-\nu^2}$ for plane stress problems.

Let the approximate finite element solution of displacement be

$$\boldsymbol{u}_h = \sum_{i=1}^{N} \Phi_i(\boldsymbol{x}) \boldsymbol{u}_h^i,$$

where $\Phi_i(\boldsymbol{x})$ is the nodal shape function containing x and y components. For implementation we usually first construct the elemental stiffness matrix and then assembly them to global stiffness matrix. We define the displacement vector on element $T \in \mathcal{T}_h$ to be $\boldsymbol{u}_{h\,T} = \{u_x^1, u_y^1, u_x^2, u_y^2, u_x^3, u_y^3\}^T$, where the subscript T denotes element T. Then the displacement of element T can be expressed as

$$\boldsymbol{u}_{h\,T}(\boldsymbol{x}) = \begin{bmatrix} \phi_{T_1} & 0 & \phi_{T_2} & 0 & \phi_{T_3} & 0 \\ 0 & \phi_{T_1} & 0 & \phi_{T_2} & 0 & \phi_{T_3} \end{bmatrix} \boldsymbol{u}_{hT},$$

where ϕ_{T_1}, ϕ_{T_2} and ϕ_{T_3} are the shape functions in element T, and with (26) the approximate strain in element T is obtained as

$$\boldsymbol{\varepsilon}_{h\,T} = \boldsymbol{R}\boldsymbol{u}_{h\,T}, \tag{27}$$

in which

$$\boldsymbol{R} = \begin{bmatrix} \dfrac{\partial \phi_{T_1}}{\partial x} & 0 & \dfrac{\partial \phi_{T_2}}{\partial x} & 0 & \dfrac{\partial \phi_{T_3}}{\partial x} & 0 \\ 0 & \dfrac{\partial \phi_{T_1}}{\partial y} & 0 & \dfrac{\partial \phi_{T_2}}{\partial y} & 0 & \dfrac{\partial \phi_{T_3}}{\partial y} \\ \dfrac{\partial \phi_{T_1}}{\partial y} & \dfrac{\partial \phi_{T_1}}{\partial x} & \dfrac{\partial \phi_{T_2}}{\partial y} & \dfrac{\partial \phi_{T_2}}{\partial x} & \dfrac{\partial \phi_{T_3}}{\partial y} & \dfrac{\partial \phi_{T_3}}{\partial x} \end{bmatrix}, \tag{28}$$

the strain energy in element T is then obtained by

$$\int_T \boldsymbol{\sigma}_{h\,T}^T \boldsymbol{\varepsilon}_{h\,T}\, d\Omega = A_T \boldsymbol{u}_{h\,T}^T \boldsymbol{R}^T \boldsymbol{E}\boldsymbol{R}\boldsymbol{u}_{h\,T},$$

where A_T is the area of element T. Therefore the element stiffness matrix is

$$\boldsymbol{K}_T = A_T \boldsymbol{R}^T \boldsymbol{E}\boldsymbol{R}.$$

With the following equation for computing the derivatives of the shape functions the implementation of the local stiffness matrix is much simplified,

$$\begin{aligned}\nabla\Phi_T &= \frac{1}{2A_T}\begin{bmatrix} y_1-y_3 & x_3-x_2 \\ y_3-y_1 & x_1-x_3 \\ y_1-y_2 & x_2-x_1 \end{bmatrix} \\ &= \begin{bmatrix} 1 & 1 & 1 \\ x_1 & x_2 & x_3 \\ y_1 & y_2 & y_3 \end{bmatrix}^{-1}\begin{bmatrix} 0 & 0 \\ 1 & 0 \\ 0 & 1 \end{bmatrix}.\end{aligned}$$

The construction of the elemental stiffness matrix in FEM is based on the element, while the construction of the local stiffness matrix for SFEM is based on the smoothing domain. The local stiffness matrix will involve contributions from all nodes that belong to the patch. For example, the smoothing domain Ω_k is in the patch $\bar{\Omega}_k$, see Fig. 1. The smoothed strain $\hat{\boldsymbol{\varepsilon}}_k$ is in fact an area weighted average strain that is

$$\begin{aligned}\hat{\boldsymbol{\varepsilon}}_k &= \frac{1}{A_k}\int_{\Omega_k}\boldsymbol{\varepsilon}(\boldsymbol{x})\,d\Omega \\ &= \frac{1}{A_k}\sum_{I=1}^{\mathcal{M}_k}\int_{\Omega_k^I}\boldsymbol{\varepsilon}_k^I(\boldsymbol{x})\,d\Omega,\end{aligned}$$

in which $\mathcal{M}_k$ is the number of elements that contain node k. For example, the smoothing domain k in Fig. 11 has 7 subdomains; Ω_k^I is a subdomain of domain k, and $\boldsymbol{\varepsilon}_k^I(\boldsymbol{x})$ is the strain in subdomain Ω_k^I. In the above equation, we do not use small i but use capital I to represent the subdomain label, in this way we will distinguish the following equations from the ones in Section 3: there the formulation is related to node i, while here the formulation is related to subdomain I. The strain energy in the smooth subdomain k

$$\begin{aligned}\int_{\Omega_k}\hat{\boldsymbol{\varepsilon}}_k^T\boldsymbol{E}\hat{\boldsymbol{\varepsilon}}_k\,d\Omega &= A_k\hat{\boldsymbol{\varepsilon}}_k^T\boldsymbol{E}\hat{\boldsymbol{\varepsilon}}_k \\ &= \frac{1}{A_k}\left(\sum_{I=1}^{\mathcal{M}_k}\int_{\Omega_k^I}\boldsymbol{\varepsilon}_k^{IT}(\boldsymbol{x})\,d\Omega\right)\boldsymbol{E}\left(\sum_{J=1}^{\mathcal{M}_k}\int_{\Omega_k^J}\boldsymbol{\varepsilon}_k^J(\boldsymbol{x})\,d\Omega\right).\end{aligned}$$

Because the shape functions are linear, $\boldsymbol{\varepsilon}_k^I(\boldsymbol{x})$ is constant over each element, and is certainly constant over Ω_k^I for it being one part of an element, thus the arguments in the above equation are omitted, and it is in a more simplified form

$$\int_{\Omega_k}\hat{\boldsymbol{\varepsilon}}_k^T\boldsymbol{E}\hat{\boldsymbol{\varepsilon}}_k\,d\Omega = \frac{1}{A_k}\sum_{I=1}^{\mathcal{M}_k}\sum_{J=1}^{\mathcal{M}_k}A_k^IA_k^J\boldsymbol{\varepsilon}_k^{IT}\boldsymbol{E}\boldsymbol{\varepsilon}_k^J, \tag{29}$$

for $I,J=1,\cdots,\mathcal{M}_k$, and $\boldsymbol{\varepsilon}_k^I$ and $\boldsymbol{\varepsilon}_k^J$ are in the form of (27), that is,

$$\begin{aligned}\boldsymbol{\varepsilon}_k^I &= \boldsymbol{R}_k^I\hat{\boldsymbol{u}}_h^I; \\ \boldsymbol{\varepsilon}_k^J &= \boldsymbol{R}_k^J\hat{\boldsymbol{u}}_h^J,\end{aligned} \tag{30}$$

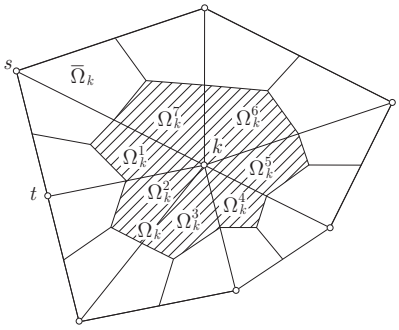

Figure 11: Illustration of patch $\bar{\Omega}_k$, smoothing domain Ω_k, and smoothing subdomains Ω_k^I.

where $\boldsymbol{R}_k^I$ and $\boldsymbol{R}_k^J$ are in the form of (28). Substituting (30) into (29) we obtain

$$\int_{\Omega_k} \hat{\boldsymbol{\varepsilon}}_k^T \boldsymbol{E} \hat{\boldsymbol{\varepsilon}}_k \, d\Omega = \frac{1}{A_k} \sum_{I=1}^{\mathcal{M}_k} \sum_{J=1}^{\mathcal{M}_k} A_k^I A_k^J \hat{\boldsymbol{u}}_h^{IT} \boldsymbol{R}_k^{IT} \boldsymbol{E} \boldsymbol{R}_k^J \hat{\boldsymbol{u}}_h^J.$$

Then we obtain the entries of local stiffness matrix in Ω_k

$$\hat{\boldsymbol{K}}_{\{I\}\{J\}(k)} = \frac{A_k^I A_k^J}{A_k} \boldsymbol{R}_k^{IT} \boldsymbol{E} \boldsymbol{R}_k^J. \tag{31}$$

Since the smoothing domain is formed by connecting the central points of element edges to the centroids of elements, we see that A_k^I is 1/3 of the element area, S_k^I, for example, area of Ω_k^1 is 1/3 of area of the element kst in Fig. 11; and A_k is 1/3 of the sum of area of all elements in $\bar{\Omega}_k$, therefore (31) is rewritten as

$$\hat{\boldsymbol{K}}_{\{I\}\{J\}(k)} = \frac{S_k^I S_k^J}{3 \sum_{l=1}^{\mathcal{M}_k} S_k^l} \boldsymbol{R}_k^{IT} \boldsymbol{E} \boldsymbol{R}_k^J. \tag{32}$$

As compared with (13) that is a 2×2 matrix, (32) is a matrix that contains 36 entries. The Matlab code for construction of the local stiffness matrix and assembly of the global stiffness matrix is listed as follows:

```
for k = 1:size(coor,1)
    [r,c,v] = find(ele == k);
    S = [];
    for m = 1:size(r,1)
        S(m) = det([1,1,1;(coor(ele(r(m),:),:))']);/2;
    end
    SumS = sum(S);
    for I = 1:size(r,1)
```

```
        vertices = coor(ele(r(I),:),:);
        II = 2*ele(r(I),[1,1,2,2,3,3])-[1,0,1,0,1,0];
        PhiGrad = [1,1,1;vertices']\[zeros(1,2);eye(2)];
        RI = zeros(3,6);
        RI([1,3],[1,3,5]) = PhiGrad';
        RI([3,2],[2,4,6]) = PhiGrad';
        for J = 1:size(r,1)
            vertices = coor(ele(r(J),:),:);
            JJ = 2*ele(r(J),[1,1,2,2,3,3])-[1,0,1,0,1,0];
            PhiGrad = [1,1,1;vertices']\[zeros(1,2);eye(2)];
            RJ = zeros(3,6);
            RJ([1,3],[1,3,5]) = PhiGrad';
            RJ([3,2],[2,4,6]) = PhiGrad';
            K(II,JJ) = K(II,JJ) + 1/3/SumS*S(I)*S(J)*RI'*E*RJ;
        end
    end
end
```

In the program, `coor` and `ele` are the data of nodes coordinates and node numbers of vertices, respectively. `II` and `JJ` are the indices expressed by $\{I\}$ and $\{J\}$ in the equations, respectively. The other part for SFEM including assembly of the right hand side and incorporation of Dirichlet conditions is the same as the procedure used in FEM, see [22].

References

[1] P. Ladevèze, D. Leguillon, Error estimate procedure in the finite element method and applications, SIAM J. Numer. Anal. 20: 485-509, 1983.

[2] R.E. Bank, A. Weiser, Some a posteriori error indicators for elliptic partial differential equations, Math. Comput. 44: 283-301, 1985.

[3] M. Ainsworth, J.T. Oden, A posteriori error estimation in finite element analysis, Comput. Methods Appl. Mech. Engrg., 142: 1-88, 1997.

[4] P. Destuynder, B. Métivet, Explicit error bounds in a conforming finite element method, Math. Comput. 68: 1379-1396, 1999.

[5] M. Paraschivoiu, J. Peraire, A.T. Patera, A posteriori finite element bounds for linear-functional outputs of elliptic partial differential equations. Comput. Methods Appl. Mech. Engrg., 150: 289-312, 1997.

[6] J. Peraire, A.T. Patera, Bounds for linear-functional outputs of coercive partial differential equations: Local indicators and adaptive refinement, Proceedings of the Workshop On New Advances in Adaptive Computational Methods in Mechanics, edited by P. Ladevèze and J.T. Oden, Elsevier 1998.

[7] S. Prudhomme, J.T. Oden, On goal-oriented error estimation for elliptic problems: application to the control of pointwise errors, Comput. Methods Appl. Mech. Engrg., 176: 313-331, 1999.

[8] J.T. Oden, S. Prudhomme, Goal-oriented error estimation and adaptivity for the finite element method. Comput. Math. Appl., 41: 735-756, 2001.

[9] N. Parés, J. Bonet, A. Huerta, J. Peraire, The computation of bounds for linear-functional outputs of weak solutions to the two-dimensional elasticity equations. Comput. Methods Appl. Mech. Engrg., 195: 406-429, 2006.

[10] B.F. de Veubeke, Displacement and equilibrium models in finite element method. In O.C. Zienkiewicz, G.S. Holister (Eds.), Stress Analysis, John Wiley and Sons, Chichester, 145–197, 1965.

[11] D.N. Arnold, Mixed finite element methods for elliptic problems, Comput. Methods Appl. Mech. Engrg., 82: 1-88, 1990.

[12] D.N. Arnold, R. Winther, Mixed finite elements for elasticity, Numer. Math., 92: 401-419, 2002.

[13] R.H. Gallagher, Finite element structural analysis and complementary energy, Finite Elem. Anal. Des., 13: 115-126, 1993.

[14] G.R. Liu, K. Zaw, Y.Y. Wang, B. Deng, A novel reduced-basis method with upper and lower bounds for real-time computation of linear elascity problems, Comput. Methods Appl. Mech. Engrg., 198: 269-279, 2008.

[15] G.R. Liu, G.Y. Zhang, Upper bound solution to elasticity problems: A unique property of the linearly conforming point interpolation method (LC-PIM), Int. J. Numer. Meth. Engrg, 74: 1128-1161, 2008.

[16] G.R. Liu, H. Nguyen-Xuan, T. Nguyen-Thoi, X. Xu, A novel Galerkin-like weakform and superconvergent alpha finite element method for mechanics problems using triangle meshes, J. Comput. Phys., 228: 4055-4087, 2009.

[17] J.S. Chen, C.T. Wu, S. Yoon, Y. You, A stabilized conforming nodal integration for Galerkin mesh-free methods. Int. J. Numer. Meth. Engrg., 50: 435-466, 2001.

[18] H. Nguyen-Xuan, S. Bordas, H. Nguyen-Dang, Smooth finite element methods: Convergence, accuracy and properties, Int. J. Numer. Meth. Engrg, 74:175-208, 2008.

[19] Z.C. Xuan, N. Parés, J. Peraire, Computing upper and lower bounds for the J-integral in two-dimensional linear elasticity, Comput. Methods Appl. Mech. Engrg., 195: 430-443, 2006.

[20] P. Ladevèze, J.P. Pelle, Mastering calculations in linear and nonlinear mechanics, Springer, 2005.

[21] L. Chamoin L, P. Ladevèze, Bounds on history-dependent or independent local quantities in viscoelasticity problems solved by approximate methods. Int. J. Numer. Meth. Engrg., 71: 1387-1411, 2007.

[22] J. Alberty, C. Carstensen, S.A. Funken, R. Klose, Matlab implementation of the finite element method in elascity, Computing, 69: 239-263, 2002.

MOX Technical Reports, last issues

Dipartimento di Matematica "F. Brioschi",
Politecnico di Milano, Via Bonardi 9 - 20133 Milano (Italy)

30/2009 Z. C. Xuan, T. Lassila, G. Rozza,
A. Quarteroni:
On computing upper and lower bounds on the outputs of linear elasticity problems approximated by the smoothed finite element method

29/2009 P.F. Antonietti, A. Pratelli:
Finite Element Approximation of the Sobolev Constant

28/2009 L. Gaudio, A. Quarteroni:
Spectral Element Discretization of Optimal Control Problems

27/2009 L. Mirabella, F. Nobile, A. Veneziani:
A robust and efficient conservative technique for simulating three-dimensional sedimentary basins dynamics

26/2009 M. Longoni, A.C.I. Malossi, A. Villa:
A robust and efficient conservative technique for simulating three-dimensional sedimentary basins dynamics

25/2009 P.E. Farrell, S. Micheletti, S. Perotto:
An anisotropic Zienkiewicz-Zhu a posteriori error estimator for 3D applications

24/2009 F. Di Maio, P. Secchi, S. Vantini, E. Zio:
Optimized Fuzzy C-Means Clustering and Functional Principal Components for Post-Processing Dynamic Scenarios in the Reliability Analysis of a Nuclear System

23/2009 L. Gerardo Giorda, F. Nobile, C. Vergara:
Analysis and optimization of Robin-Robin partitioned procedures in Fluid-Structure Interaction Problems

22/2009 L. Formaggia, S. Minisini, P. Zunino:
Modeling erosion controlled drug release and transport phenomena in the arterial tissue

21/2009 L. Bonaventura, S. Castruccio, L.M. Sangalli:
A Bayesian approach to geostatistical interpolation with flexible variogram models